BBA - Biomembranes 1866 (2024) 184291

Contents lists available at ScienceDirect

BBA - Biomembranes

journal homepage: www.elsevier.com/locate/bbamem

Use of bacterial photosynthetic vesicles to evaluate the effect of ionic liquids on the permeability of biological membranes

Tancredi Bin [a], Giovanni Venturoli [a,b], Anna Maria Ghelli [a], Francesco Francia [a,*]

[a] Department of Pharmacy and Biotechnology, University of Bologna, Via Irnerio 42, 40126 Bologna, Italy
[b] Consorzio Nazionale Interuniversitario per le Scienze Fisiche della Materia (CNISM), c/o Dipartimento di Fisica e Astronomia (DIFA), via Irnerio 46, Università di Bologna, I-40126 Bologna, Italy

ARTICLE INFO

Keywords:
Ionic liquids
NTf_2
Rhodobacter Capsulatus
Chromatophores
Carotenoid shift
Membrane potential

ABSTRACT

Ionic liquids (ILs) are salts composed of a combination of organic or inorganic cations and anions characterized by a low melting point, often below 100 °C. This property, together with an extremely low vapor pressure, low flammability and high thermal stability, makes them suitable for replacing canonical organic solvents, with a reduction of industrial activities impact on the environment. Although in the last decades the eco-compatibility of ILs has been extensively verified through toxicological tests performed on model organisms, a detailed understanding of the interaction of these compounds with biological membranes is far from being exhaustive. In this context, we have chosen to evaluate the effect of some ILs on native membranes by using chromatophores, photosynthetic vesicles that can be isolated from *Rhodobacter capsulatus*, a member of the purple non-sulfur bacteria. Here, carotenoids associated with the light-harvesting complex II, act as endogenous spectral probes of the transmembrane electrical potential ($\Delta\Psi$). By measuring through time-resolved absorption spectroscopy the evolution of the carotenoid band shift induced by a single excitation of the photosynthetic reaction center, information on the $\Delta\Psi$ dissipation due to ionic currents across the membrane can be obtained. We found that some ILs cause a rather fast dissipation of the transmembrane $\Delta\Psi$ even at low concentrations, and that this behavior is dose-dependent. By using two different models to analyze the decay of the carotenoid signals, we attempted to interpret at a mechanistic level the marked increase of ionic permeability caused by specific ILs.

1. Introduction

The increased demand for large-scale chemical processes with low environmental impact has led to a growing interest in the development of new eco-friendly compounds. In this context, ionic liquids (ILs) have attracted the attention of industrial chemistry as potential substitutes for canonical organic solvents due to their physicochemical properties such as very low vapor pressure, low flash point, low melting point, a wide electrochemical window and the ease of separation from reactants and products of chemical reactions [1]. ILs are composed of organic or inorganic cations and anions easily interchangeable with each other [2], allowing their properties to be adapted to a wide range of chemical reactions. Over the past decades, an enormous amount of scientific data has been accumulated on the potential use of ILs in different processes [3,4], alongside with an extensive literature on their effects on living organisms. These latter studies have mainly been conducted on model organisms to test the ecotoxicity of several ILs [5,6], while very little information is available on their specific interaction with biological membranes. Furthermore, the interaction of ILs with membranes has been studied almost exclusively on liposomes [7], i.e. on in vitro reconstituted systems mimicking the natural lipidic bilayer but in the absence of proteins and specifically in the absence of protein complexes devoted to the building up of the transmembrane electrical potential in membrane systems carrying on fundamental bioenergetic processes. Only recently, photosynthetic membrane vesicles (chromatophores) from purple bacteria have been exploited as a useful model system to study the effect of ionic liquids on a native biological membrane [8,9].

Chromatophores (Chr) are bioenergetically active vesicles easily isolated from photosynthetic bacteria that have been extensively characterized [10] and widely used to evaluate the effects of exogenous compounds on membrane integrity [11,12]. All the components of the photosynthetic apparatus responsible for the transduction of radiant energy into chemical energy are functionally present in this native vesicular system. Their function is now well known at the molecular level

* Corresponding author.
E-mail address: francesco.francia@unibo.it (F. Francia).

https://doi.org/10.1016/j.bbamem.2024.184291
Received 12 October 2023; Received in revised form 22 January 2024; Accepted 24 January 2024
Available online 30 January 2024

and their structure determined at atomic resolution [13–21]. In *Rhodobacter* (*Rb.*) *capsulatus*, a representative member of the purple non-sulfur bacteria, primary photochemistry is triggered by the absorption of radiant energy by the light-harvesting complexes LH2 and LH1. Both of these antenna complexes have a similar architecture, being made up of heterodimers of α and β subunits, single transmembrane helices that bind molecules of bacteriochlorophyll and carotenoids. The αβ heterodimers build circular structures that keep photosynthetic pigments in the correct orientation for efficient excitation energy transfer. The LH2 complex consists of 8–9 heterodimers and is located peripherally to LH1, which forms a larger structure surrounding the photochemical reaction center (RC). The RC consists of two pseudo-symmetric L and M membrane subunits and one H subunit with a large cytoplasmatic domain anchored to the LM complex by a single hydrophobic helix. The RC protein moiety holds the pigment cofactor tree, formed by two symmetrical branches originating from a special pair (P) of bacteriochlorophylls located in the vicinity of the periplasmic side of the membrane and extending in sequence to two accessory bacteriochlorophylls, two bacteriopheophytins and two binding sites for quinone molecules, located close to the cytoplasmic side of the membrane, referred to as Q_A and Q_B. Following excitation, the RC special pair P delivers an electron to one of the bacteriopheophytins, initiating an electron transfer chain which leads to the sequential reduction of the quinone molecules located at the Q_A and Q_B site (see Fig. 1). After double reduction and protonation, the quinol bound at Q_B leaves the site and oxidizes at the Qo site of a ubiquinol-cytochrome *c* oxido-reductase (bc_1 complex). Protons are released on the periplasmic side, while electrons, following a well-defined Q-cycle mechanism, reduce a soluble cytochrome c_2 molecule and a quinone molecule located in the Qi site of the bc_1, facing the cytoplasmic side of the complex. The reduced cytochrome c_2 is the electron donor of the photoxidized special pair P of the RC [22,23]. This light-driven cyclic electron flow (Fig. 1), according to Mitchell's chemiosmotic theory, acts as a redox pump generating a proton gradient ultimately used by ATP synthase to form ATP [24]. Through this system, the light energy is initially transduced into an electrochemical concentration gradient of protons across the membrane, expressed by Mitchell as proton motive force [25], which consists of an electrical (ΔΨ) and a pH (ΔpH) component.

A prerequisite for further transduction of the proton gradient into chemical energy in the form of ATP is membrane integrity, since increased ion diffusion (dissipating ΔΨ) or proton leakage (affecting both ΔΨ and ΔpH) will decrease the proton motive force leading to a decrease in the overall performance of the system.

The carotenoids bound to the LH2 antenna complex respond to the transmembrane electric field generated by the photoinduced RC charge separation and by the other electrogenic events of the photoactivated electron transfer chain with a shift towards the red of their absorption spectrum [26]. Since the amplitude of this absorbance variation is linearly related to the magnitude of the transmembrane potential ΔΨ, these pigments act as an endogenous voltmeter and allow to follow spectrophotometrically the onset of ΔΨ generated by photoactivation of the chromatophores and its subsequent decay in the dark due to ionic currents through the membrane [27].

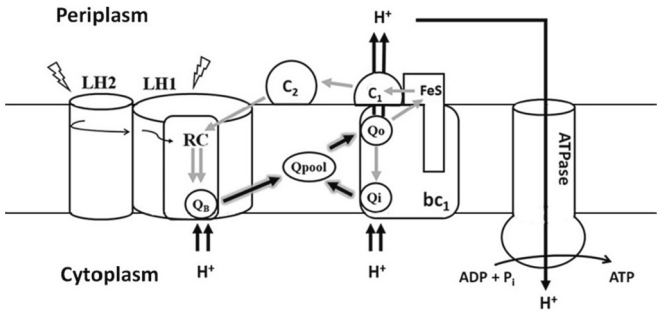

Fig. 1. Cartoon of light-induced electron transfer in the photosynthetic membrane of *Rb. capsulatus*. LH2, light harvesting complex II; LH1, light harvesting complex I; RC, reaction center; Q_B, RC quinone binding site; bc_1, ubiquinol-cytochrome *c* oxidoreductase; FeS, Rieske protein iron sulfur cluster; c_1, cytochrome c_1; Qo, quinol oxidation site of bc_1; Qi, quinone reduction site of bc_1; c_2, cytochrome c_2; ATPase, ATP synthase complex. Black thin arrows indicate energy transfer within the LH2-LH1-RC complex; black thick arrows represent proton movement; gray thick arrows indicate electron transfer.

In this work, we have used this approach to investigate the influence of five ILs with promising application in electrochemistry (highlighted in gray in Fig. 2) on the membrane potential of chromatophores, by monitoring the decay in the dark of the carotenoid band shift induced by a short flash of light. We found that bis(trifluoromethylsulfonyl)imide (NTf_2) containing compounds induce rapid membrane potential dissipation even at low (μM) concentrations. Our results indicate that chromatophore vesicles represent an ideal system to investigate at the molecular level the effects of different ILs on native biological membranes.

2. Materials and methods

2.1. Chemicals

The following Ionic Liquids were purchased from IoLiTech Gmbh (Heilbronn, Germany): butyltriethylammonium-bis(trifluoromethyl sulfonyl)imide (N2224-NTf_2); 1-Butyl-1-methylpyrrolidinium-bis(trifluoromethylsulfonyl)imide (BMPyrr-NTf_2); 1-butyl-1-methylpyrrolidinium-chloride (BMPyrr-Cl); Choline-bis(trifluoromethylsulfonyl)imide (Chol-NTf_2); 1-Ethyl-3-methylimidazolium-bis(trifluoromethylsulfonyl) imide (c_1c_2 Im-NTf_2); 1-Ethyl-3-methylimidazolium-trifluoromethanesulfonate (c_1c_2 Im-OTf); 1-Ethyl-3-methylimidazolium tetrafluoroborate (c_1c_2 Im-BF_4); 1-Ethyl-3-methylimidazolium chloride (c_1c_2 Im-Cl).

Choline chloride (Chol-Cl) was purchased from Sigma-Aldrich.

2.2. Bacterial growth and chromatophores isolation

Rb. Capsulatus cells (strain MT1131 [28]) were photosynthetically grown in MPYE medium (3 g/L Peptone, 3 g/L yeast extract, 1.6 mM $MgCl_2$, 1 mM $CaCl_2$, pH 7), harvested in the late log phase, and frozen at −80 °C. To isolate Chr vesicles, the thawed cells were washed extensively in 50 mM MOPS buffer, pH 7.3 in order to remove any traces of MPYE medium; cells were subsequently resuspended in the same buffer, and treated with a French Press at 1000 psi. Unbroken cells and cell debris were removed by centrifugation at 27,000*g* for 35 min at 4 °C and Chr were isolated by ultracentrifugation of the supernatant at 200,000 *g* for 90 min at 4 °C. The Chr pellet was resuspended in 50 mM MOPS buffer, pH 7.3, partitioned into 100 μL aliquots, flash frozen in liquid nitrogen and stored at −80 °C.

To estimate the total bacteriochlorophyll (BChl) content of the Chr preparation, 5–10 μL of vesicles suspension were extracted with 1 mL cold mixture of acetone:methanol 7:2; the BChl concentration was evaluated from the absorption at 772 nm using a molar extinction coefficient of 75 mM^{-1} cm^{-1} [29].

2.3. Visible absorption spectroscopy and data analysis

The time evolution of the carotenoid band shift after a single xenon flash (of less than 8 μs duration) was followed at 503 nm by using a kinetic spectrophotometer of local design [30]. Two Wratten 88 A gelatin filters were placed in front of the xenon lamp, producing photoexciting radiation with wavelength longer than 700 nm. An optical guide, perpendicular to the direction of the measuring beam, was used to direct the exciting light onto the sample; the photomultiplier was protected from the scattered light of the sample by a Corning 4–96 filter. Data acquisition was via a LeCroy 9361C digital oscilloscope interfaced with a PC.

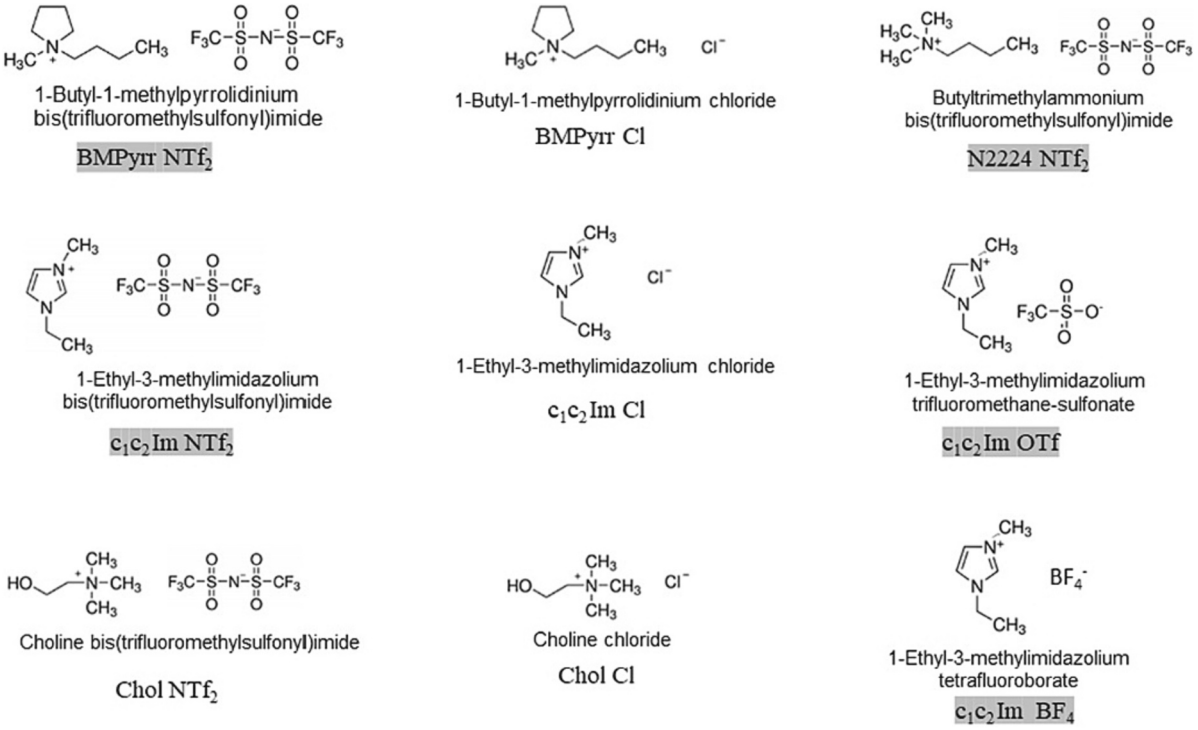

Fig. 2. Molecular structure of the ILs tested in this study with the adopted abbreviations.

Chromatophores were suspended in 50 mM MOPS, pH 7.3, at a BChl concentration kept fixed at 70 μM. Antimycin A and oligomycin were added at 10 μM; 1 mM KCN was also added to inhibit any residual cytochrome *c* oxidase activity. The redox potential of the samples was kept in a range between 100 and 150 mV by adding 1 mM Na-ascorbate. In order to maximize the excitation of the chromatophore reaction center and ensure mixing of the added ILs during the titrations, the samples were placed in a Hellma quartz cuvette (Hellma GmbH, Müllheim, Germany) with an excitation path length of 4 mm, a measuring beam path length of 1 cm and a conical flare at the bottom which housed a magnetic stirrer.

The total amount of RCs photoexcited in our measurements was estimated from the absorbance change (ΔA) induced at 542 nm by the xenon actinic pulse using a Δε of 10.3 mM^{-1} cm^{-1} [31]. In these measurements, the flash-induced ΔΨ was rapidly collapsed by adding 10 μM valinomycin in Chr suspended in 30 mM KCl, 50 mM MOPS, pH 7.3, thus avoiding the spectral interference of electrochromic contributions at 542 nm. The rapid, unresolved re-reduction of photoxidized P by the pre-reduced cytochrome c_2 was prevented by fixing the redox potential at 415 mV through the addition of 0.5 mM ferro/ferri-cyanide. The amount of RC photoxidized at lower potential (i.e. under the conditions of carotenoid shift measurements) was calculated using the Nernst equation and a midpoint redox potential (Em) of 440 mV for the P^+/P semi-couple [32]. Non-linear curve fits of the carotenoid band shift decay kinetics were performed with the Origin 6.1 software.

3. Results

3.1. Kinetics of the carotenoid shift decay in the presence of ILs

The kinetics of the carotenoid shift signal, induced by a short (microsecond) light excitation on a suspension of chromatophores, is shown in Fig. 3, trace a. The rapid and unresolved ΔA increase, in the microsecond time scale, is due to the generation of the ΔΨ by the electron and proton transfer steps localized in the RC (see Introduction) [33,34]. To better estimate the instantaneous decay of ΔΨ from the kinetic traces, the carotenoid signals have been measured in the presence of antimycin, an inhibitor that blocks much of the electron transfer activity of the cytochrome bc_1 complex, whose contribution to the carotenoid shift [35] takes place in a few milliseconds. The possible leakage of protons from damaged ATPase was prevented by adding oligomycin, a specific inhibitor of the translocation of H^+ through the F_0 channel of ATP synthase [36]. Under these conditions, the decay of the carotenoid signal is essentially determined by the ion fluxes through the lipid bilayer, providing quantitative information on the permeability properties of the membrane.

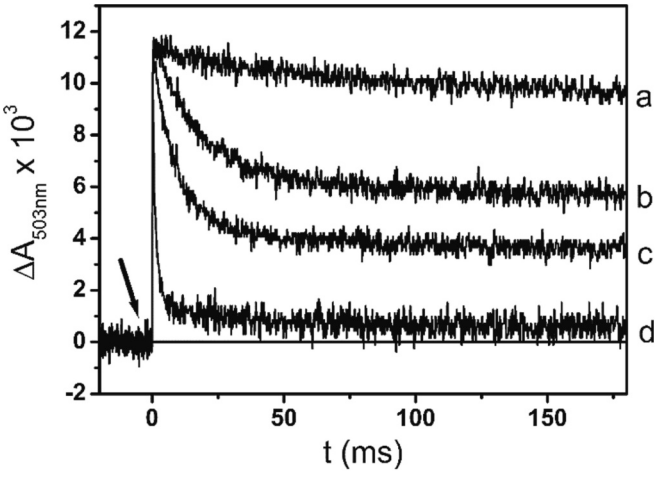

Fig. 3. Kinetic traces of the carotenoid shift signal induced by a single turnover flash, recorded at 503 nm in a Chr suspension at increasing concentration of BMPyrr NTf_2: a, control; b, 5 μM; c, 20 μM; d,500 μM. The arrow indicates the excitation of the sample with the actinic flash (at time $t = 0$).

Fig. 3 shows the kinetics of the carotenoid shift signal induced by a single flash in chromatophores supplemented with antimycin and oligomycin, in the presence of increasing concentrations of the ionic liquid

$BMPyrr\text{-}NTf_2$ (traces b,c,d).

In the absence of the IL (trace a) the decay is very slow (on the timescale of seconds) indicating an extremely low intrinsic permeability of the Chr membrane to ions. $BMPyrr\text{-}NTf_2$ dramatically accelerates the decay (traces b-d), even at very low (μM) concentrations, indicating that this IL greatly promotes the dissipation of the membrane potential.

Interestingly, the decay kinetics in the presence of the IL are strongly biphasic, with a fast phase amplitude that increases with increasing IL concentration and a tail which decays very slowly, on the timescale of the control. Such a pronounced biphasicity has been previously observed by us in a study [8] of the effects of imidazolinium and pyrrolidinium ILs, with chloride or dicyanamide as counter anions, on the decay of the carotenoid shift following a single turnover flash in chromatophores. In this study, the observed non-homogeneous kinetics of the carotenoid shift decay could be satisfactorily described by a statistical model originally developed by Schmid and Junge [37] to explain a similar biphasic decay of the carotenoid shift induced by uncouplers in thylakoid membranes. The model is based on the idea that the strongly non-homogeneous decay of the carotenoid signal observed in the presence of ILs reflects a Poisson distribution of permeating ions over the whole chromatophore population. Under this assumption an analytical expression can be obtained for the decay of ΔΨ and correspondingly of the carotenoid signal (for a detailed derivation see Ref. [8], i.e.:

$$\Delta A(t) = \Delta A(0) \bullet e^{-m-k_l \bullet t} \bullet e^{m \bullet e^{-k \bullet t}} \quad (1)$$

where ΔA(0) is the maximum amplitude of the carotenoid shift immediately after the excitation flash, m is the average number of permeating ions per vesicle, k_l represents a rate constant describing the intrinsic background ion leak of the membrane in the absence of ILs, and k a rate constant (conductance) for an individual ion of the specific permeant species tested. In a first attempt to account for the inhomogeneous decays observed in the presence of the ILs tested in the present study we have adopted this statistical model. Fig. S1 shows that Eq. (1) provides an accurate fit of the non-homogeneous carotenoid signal decays recorded for the whole set of ILs examined. The correspondent values of the best fitting parameters (m, k_l, k) are reported in Table S1. It has to be noticed that in our previous study [8], aimed at elucidating how the polarity of the alkyl side chain present on imidazole or pyrrolidine cations influences the permeability of ILs, the carotenoid signal decays recorded at increasing concentration of the examined ILs could be accounted for by global fitting to Eq. (1) with a common k value for any individual IL (i.e. the same ion-specific rate constant at any concentration). This global fit approach gave unsatisfactory results when applied to the data obtained in the presence of the ILs tested in the present study (not shown). Accurate fit to Eq. (1) could be obtained only when the parameter k was allowed to be varied at the different concentration of the IL examined. As shown in Table S1, excluding Chol-Cl, a non-permeant ionic liquid often used as control in bioenergetic studies [38], for all the ILs examined best fitting to Eq. (1) resulted in k values increasing at increasing IL concentrations by approximately one order-of-magnitude over the concentration range tested. Additionally, Table S1 shows that the average number of permeating ions per vesicle (m) tends to saturate to a very low value (around 2). These two outcomes of the statistical model summarized by Eq. (1) are not easily interpreted in terms of the known physical properties of the chromatophore system (see Discussion), and have led us to consider an alternative model to account for the biphasic decay of the transmembrane potential probed by the carotenoid shift. Such a model was originally developed to explain the biphasic decay of the membrane potential due to permeation of hydrophobic ions and ionophores through artificial lipid bilayer membranes in charge-pulse experiments [39,40]. It relies on the largely accepted idea that the permeating ion is located in deep potential energy minima at the membrane solution-interfaces and that the overall ion transport occurs in three consecutive steps: adsorption of the ion from water to the interface, translocation across the central energy barrier to the opposite interface (rate constant k_i), and desorption into the aqueous phase (rate constant k_{ma}). It can be demonstrated [39] that, for sufficiently small transmembrane potentials, i.e. $\Delta\psi << RT/F$, being R, T and F the gas constant, absolute temperature, and Faraday constant respectively, for a symmetric membrane characterized by deep potential energy minima at the water-membrane interfaces and by a high central barrier of arbitrary shape, the decay of the transmembrane potential Δψ(t), measured in our case by the decay of the carotenoid absorbance change ΔA(t), assumes the form

$$\Delta\psi(t) = \Delta\psi(0)\left(a_1 e^{-t/\tau_1} + a_2 e^{-t/\tau_2}\right) \quad (2)$$

where Δψ(0) is the initial transmembrane potential, given in our case by the absorbance change ΔA(0) immediately after the excitation flash.

Fig. 4 and Fig. S2 show that fitting to Eq. (2) provides an accurate description of the carotenoid shift decay for all the IL examined at all concentrations tested. The corresponding values of the best fitting parameters (a_1, τ_1, τ_2) are reported in Table 1. Goodness of fit is comparable to that obtained by fitting the same set of kinetics to Eq. (1).

According to the model developed by Benz et al. [39] the relaxation times τ_1, τ_2 and the relaxation amplitude a_1 can be expressed in terms of the kinetic rate constants k_i and k_{ma}, governing the translocation across the central energy barrier and desorption into the aqueous phase, respectively, and of the total interfacial ion concentration N_t (pmol · cm^{-2}). For $k_{ma} << k_i$, a condition which is generally satisfied when the two relaxation times τ_1 and τ_2 are distinctly separated, this relationship is approximated by the following equations

$$\tau_1 \approx \frac{1}{2\,k_i(1+\alpha^2 b N_t)} \quad (3)$$

$$\tau_2 \approx \frac{1+\alpha^2 b N_t}{k_{ma} b N_t} \quad (4)$$

$$a_1 \approx \frac{\alpha^2 b N_t}{1+\alpha^2\, b\, N_t} \quad (5)$$

where α is the fraction of the total membrane potential Δψ dropping across the central energy barrier and b is related to the membrane capacitance C_m and to the valency z of the permeating ion by

$$b = \frac{z^2 F^2}{4RTC_m} \quad (6)$$

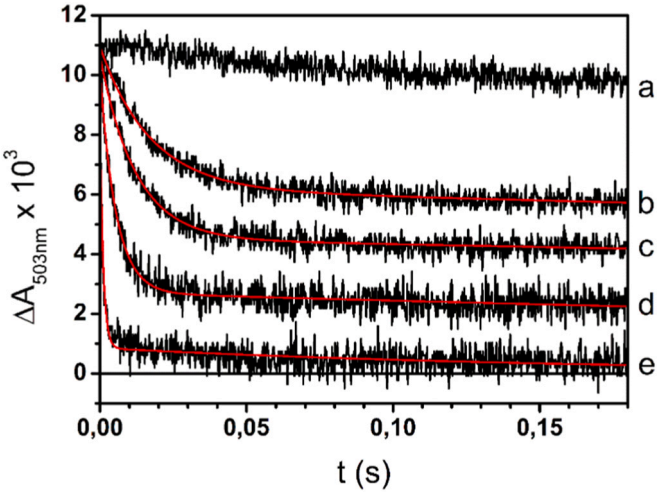

Fig. 4. Kinetics of the carotenoid signal decay following a single turnover flash recorded at 503 nm in a Chr suspension at increasing concentrations of $N2224\text{-}NTf_2$: a, control; b, 5 μM; c, 10 μM; d, 50 μM, e, 1 mM. Red lines represent best fit to Eq. (2). (For interpretation of the references to colour in this figure legend, the reader is referred to the web version of this article.)

Table 1
Values of the parameters (τ_1, τ_2, a_1) obtained by fitting the decay kinetics of the carotenoid shift signal to Eq. (2) ($a_2 = 1\text{-}a_1$) and the corresponding values of k_i and N_t, calculated using Eqs. (9) and (10) (see text for details).

c (μM)	τ_1 (s) · 10^3	τ_2 (s)	a_1	k_i (s^{-1})	N_t (pmol ·cm^{-2})
$N2224NTf_2$					
5	17.25 ± 0.47	2.33 ± 0.30	0.4344 ± 0.0040	16.39 ± 0.46	0.449 ± 0.007
10	12.18 ± 0.27	2.31 ± 0.33	0.5736 ± 0.0036	17.50 ± 0.41	0.787 ± 0.011
20	8.42 ± 0.17	1.17 ± 0.09	0.6433 ± 0.0032	21.18 ± 0.47	1.055 ± 0.015
50	5.46 ± 0.16	0.96 ± 0.11	0.7302 ± 0.0044	24.71 ± 0.83	1.583 ± 0.036
100	3.30 ± 0.11	0.62 ± 0.06	0.8146 ± 0.0041	28.09 ± 1.12	2.571 ± 0.069
200	2.29 ± 0.08	0.41 ± 0.04	0.8621 ± 0.0038	30.11 ± 1.35	3.657 ± 0.118
500	1.41 ± 0.07	0.23 ± 0.02	0.8802 ± 0.0045	42.48 ± 2.65	4.298 ± 0.184
1000	1.11 ± 0.06	0.16 ± 0.01	0.8963 ± 0.0048	46.29 ± 3.28	5.057 ± 0.263
BMPyrr NTf_2					
5	17.13 ± 0.43	1.96 ± 0.22	0.4669 ± 0.0039	15.56 ± 0.41	0.512 ± 0.008
10	11.96 ± 0.25	1.26 ± 0.09	0.5529 ± 0.0034	18.69 ± 0.42	0.724 ± 0.010
20	9.38 ± 0.18	1.14 ± 0.08	0.6220 ± 0.0031	20.15 ± 0.42	0.963 ± 0.013
100	3.43 ± 0.08	0.48 ± 0.02	0.8030 ± 0.0029	28.71 ± 0.79	2.385 ± 0.044
200	2.56 ± 0.09	0.37 ± 0.03	0.8585 ± 0.0040	27.64 ± 1.25	3.549 ± 0.116
500	1.40 ± 0.06	0.21 ± 0.02	0.8847 ± 0.0041	41.19 ± 2.29	4.487 ± 0.180
1000	1.03 ± 0.06	0.23 ± 0.02	0.8957 ± 0.0048	50.65 ± 3.77	5.022 ± 0.259
c_1c_2 Im NTf_2					
5	15.55 ± 0.43	1.64 ± 0.11	0.3616 ± 0.0036	20.53 ± 0.58	0.331 ± 0.005
10	11.65 ± 0.25	1.61 ± 0.10	0.4587 ± 0.0032	23.23 ± 0.52	0.496 ± 0.006
20	8.47 ± 0.17	1.32 ± 0.07	0.5306 ± 0.0031	27.71 ± 0.59	0.661 ± 0.008
50	5.98 ± 0.12	1.06 ± 0.05	0.6150 ± 0.0031	32.19 ± 0.69	0.934 ± 0.012
100	3.93 ± 0.08	0.89 ± 0.05	0.7276 ± 0.0029	34.65 ± 0.79	1.563 ± 0.023
200	2.36 ± 0.08	0.70 ± 0.08	0.8332 ± 0.0037	35.34 ± 1.43	2.922 ± 0.078
500	1.36 ± 0.05	0.32 ± 0.02	0.8764 ± 0.0037	45.46 ± 2.15	4.146 ± 0.140
1000	1.10 ± 0.06	0.30 ± 0.03	0.8885 ± 0.0045	50.70 ± 3.43	4.660 ± 0.210
c_1c_2 Im BF_4					
100	31.30 ± 2.86	1.78 ± 0.23	0.1747 ± 0.0084	13.19 ± 1.21	0.124 ± 0.007
200	30.28 ± 1.90	1.68 ± 0.23	0.2537 ± 0.0081	12.32 ± 0.78	0.199 ± 0.009
400	30.01 ± 1.40	2.66 ± 0.60	0.3309 ± 0.0077	11.14 ± 0.54	0.289 ± 0.010
$1 \cdot 10^3$	22.56 ± 0.70	2.28 ± 0.38	0.4352 ± 0.0053	12.51 ± 0.41	0.451 ± 0.010
$2 \cdot 10^3$	14.15 ± 0.30	1.24 ± 0.10	0.5535 ± 0.0036	15.77 ± 0.36	0.725 ± 0.010
$5 \cdot 10^3$	9.34 ± 0.17	0.98 ± 0.07	0.6796 ± 0.0031	17.13 ± 0.35	1.241 ± 0.017
$1 \cdot 10^4$	6.32 ± 0.12	0.65 ± 0.04	0.7658 ± 0.0029	18.53 ± 0.42	1.913 ± 0.031
$2 \cdot 10^4$	4.38 ± 0.10	0.41 ± 0.02	0.8215 ± 0.0029	20.38 ± 0.57	2.692 ± 0.054
$5 \cdot 10^4$	2.64 ± 0.10	0.24 ± 0.02	0.8751 ± 0.0041	23.66 ± 1.19	4.098 ± 0.155
$9 \cdot 10^4$	1.67 ± 0.07	0.24 ± 0.02	0.8801 ± 0.0043	35.89 ± 1.98	4.294 ± 0.175
$18 \cdot 10^4$	1.47 ± 0.07	0.29 ± 0.02	0.8572 ± 0.0050	48.56 ± 2.87	3.512 ± 0.144
c_1c_2 Im OTf					
5	73.98 ± 24.18	17.82 ± 2.85	0.1569 ± 0.0543	5.70 ± 1.90	0.109 ± 0.045
20	47.48 ± 6.11	5.71 ± 1.20	0.1805 ± 0.0176	8.63 ± 1.13	0.129 ± 0.015
100	36.65 ± 3.67	2.55 ± 0.57	0.1754 ± 0.0106	11.25 ± 1.14	0.124 ± 0.009
$1 \cdot 10^3$	21.79 ± 0.69	1.75 ± 0.17	0.3642 ± 0.0046	14.59 ± 0.47	0.335 ± 0.007
$5 \cdot 10^3$	9.11 ± 0.17	0.88 ± 0.05	0.6518 ± 0.0030	19.11 ± 0.39	1.095 ± 0.014
$2 \cdot 10^4$	4.19 ± 0.12	0.43 ± 0.03	0.8091 ± 0.0038	22.78 ± 0.79	2.480 ± 0.061
$5 \cdot 10^4$	2.34 ± 0.08	0.22 ± 0.01	0.8690 ± 0.0040	27.99 ± 1.29	3.881 ± 0.137
$9 \cdot 10^4$	1.75 ± 0.07	0.22 ± 0.01	0.8668 ± 0.0042	38.06 ± 1.94	3.807 ± 0.139
$18 \cdot 10^4$	1.22 ± 0.06	0.29 ± 0.02	0.8590 ± 0.0044	57.80 ± 3.36	3.563 ± 0.129
Chol Cl					
$1 \cdot 10^3$	63.39 ± 19.28	3.82 ± 2.80	0.1199 ± 0.0354	6.94 ± 2.13	0.080 ± 0.027
$5 \cdot 10^3$	48.06 ± 5.94	9.95 ± 1,49	0.1804 ± 0.0168	8.53 ± 1.07	0.129 ± 0.015
$1 \cdot 10^4$	33.68 ± 2.78	2.57 ± 0.47	0.1826 ± 0.0082	12.13 ± 1.01	0.131 ± 0.007
$2 \cdot 10^4$	32.12 ± 2.22	2.56 ± 0.43	0.2007 ± 0.0073	12.44 ± 0.87	0.147 ± 0.007
$5 \cdot 10^4$	36.52 ± 2.75	3.26 ± 0.87	0.2137 ± 0.0095	10.77 ± 0.82	0.159 ± 0.009
$9 \cdot 10^4$	33.84 ± 2.80	1.81 ± 0.22	0.1708 ± 0.0079	12.25 ± 1.02	0.120 ± 0.007
$18 \cdot 10^4$	33.08 ± 2.95	1.78 ± 0.19	0.1446 ± 0.0070	12.93 ± 1.16	0.100 ± 0.006
$40 \cdot 10^4$	36.68 ± 3.78	1.64 ± 0.18	0.1381 ± 0.0087	11.72 ± 1.21	0.094 ± 0.007

By combining Eqs. (3)–(5) a simple relationship can be obtained for k_i which is independent of α, b and N_t. From Eq. (4) we have $\alpha^2 = k_{ma}\tau_2 - 1/bN_t$ which can be replaced in Eqs. (3) and (5), obtaining.

$$\tau_1 = 1/(2\, k_i\, k_{ma}\, \tau_2\, b\, N_t) \quad (7)$$

and

$$a_1 = 1 - 1/(k_{ma}\, \tau_2\, b\, N_t) \quad (8)$$

From Eq. (7) we have $b\, N_t = 1\, /\, (2\, k_i\, k_{ma}\, \tau_2\, \tau_1)$ which can be replaced in Eq. (8) obtaining.

$$k_i = (1 - a_1)/(2\, \tau_1) \quad (9)$$

Eq. (9) is particularly useful because it allows to evaluate the rate constant k_i for translocation of the ion through the central energy barrier of the membrane starting simply from the experimental values of the relaxation amplitude a_1 and time τ_1 of the fast phase. Eq. (9) makes also clear that the fast component of the membrane potential decay (see Eq. (2)) arises essentially from the ion translocation across the central barrier.

In order to obtain information on the partition of the ion into the membrane (i.e. on the interfacial surface concentration of the ion, N_t), from Eq. (5) we obtain

$$N_t = \frac{a_1}{\alpha^2 b(1-a_1)} \tag{10}$$

The parameter b in Eq. (10) has been estimated by using Eq. (6), with the value $C_m = 5.5 \cdot 10^{-3}$ F m^{-2} determined experimentally for the chromatophore membrane [41] and $\alpha^2 \approx 1$ has been set in Eq. (10). This may appear a rather crude approximation, but it allows a reasonable, basic estimate of N_t from the experimentally determined values of a_1, when considering that for most of the artificial bilayer membranes studied α has been found close to unity [39] except for a value of 0.75 reported in [42]. Values of k_i and N_t obtained as described above (Eqs. (9) and (10)) are collected in Table 1. In principle, according to the model, if adsorption of the IL has no significant effect on the membrane structure, the value of k_i for a given IL is supposed to be independent of the concentration. At variance, for all the IL tested the calculated k_i increases progressively upon increasing the IL concentration (Table 1). However the increase in k_i appears to be systematically more limited (smaller by a factor of ~3) when compared to the correspondent increase of the rate constant k of the statistical model, obtained by fitting the carotenoid shift decay to Eq. (1) (cf. Table 1 with Table S1). The values obtained for the total adsorbed surface concentration, N_t, increase as expected upon increasing the IL concentration, but reveal a saturation behavior, consistent with what found for hydrophobic ions in artificial lipid bilayer, studied by charge pulse relaxation [39]. Moreover, when considering the average dimension of the chromatophore vesicles and the relative contents of lipids and proteins (see Discussion), the values at which N_t saturates appear to be much more reasonable than the saturation values of the average number m of permeating ions calculated from the statistical model (Eq. (1)). Based on these arguments, developed more extensively in the Discussion, we believe that the model summarized in Eqs. (2)–(6) provides a more consistent and physically meaningful approach when analyzing the decay of the membrane potential following an excitation flash of light.

Noteworthy, inspection of Table 1, shows that in all the NTf_2-containing ILs (N2224-NTf_2, BMPyrr-NTf_2, c_1c_2Im-NTf_2) the increase of k_i and N_t titrates at concentrations more than two order-of-magnitude lower as compared to c_1c_2In-OTf and c_1c_2Im-BF_4, suggesting that the NTf_2^- anion is much more prone to be adsorbed to and to permeate the chromatophore membrane as compared to other ions.

3.2. The increase of membrane ionic current in the presence of ILs

As stated above, it has been shown that the amplitude of the carotenoids shift signal (ΔA) is linearly related to the chromatophore membrane potential [27], implying that the change in ΔΨ due to dissipative ionic currents can be monitored by following the change of the carotenoid signal ΔA in time following charge separation elicited by the flash. Assuming a constant value of the membrane capacitance C_m, ΔΨ is related to the amount Q of separated charge by $\Delta\Psi = Q / C_m$. The overall ionic current j, responsible of ΔΨ dissipation, is therefore given by $j = dQ / dt = C_m\, d\Delta\Psi / dt$, and, in terms of the carotenoid signal, ΔA:

$$j \approx \frac{d\Delta A}{dt} \tag{11}$$

In order to compare the efficacy of the different ILs tested in dissipating ΔΨ we have evaluated the overall ionic current from the initial rapidity $r(0)$ of the carotenoid signal decay immediately after the flash. This parameter is model independent and since both the statistical model (Eq. (1)) and the model leading to a biexponential decay (Eq. (2)) provide a very accurate fit of the carotenoid shift decay, very similar results will be obtained by considering the first derivative of Eq. (1) or of Eq. (2) at time 0 and changing its sign. In the following, we show the results obtained by using Eq. (2), i.e.

$$r(0) = \Delta A(0) \bullet (a_1/\tau_1 + a_2/\tau_2) \tag{12}$$

Accurate values of $r(0)$ have been obtained by substituting into Eq. (12) the values of the parameters $\Delta A(0)$, a_1, $a_2 = 1\text{-}a_1$, τ_1, τ_2 yielded by fitting the carotenoid signal decays to Eq. (2) (see Table 1). Values of $r(0)$ can be converted to a zero time ionic current across the chromatophore membrane expressed as electrons translocated per bacteriochlorophyll (BChl) per unit time (e$^-$ BChl^{-1} s^{-1}) [8,43]. Under our experimental conditions the contribution to the carotenoids band shift is solely due to flash-induced charge separations within the RC, implying that the observed amplitude of $\Delta A(0)$ measures the ΔΨ generated by the displacements across the lipid bilayer of a single-electron for activated RC, i.e. per primary donor P photoxidized. At a BChl concentration of 70 μM, which was kept constant in all experimental measurements, the concentration of flash-oxidized RC was $[P^+] = 210$ nM (see Materials and Methods). On this basis, $r(0)$ values can be converted into j_0 values (e$^-$ BChl^{-1} s^{-1}) calculated as:

$$j_0 = \frac{r(0) \bullet [P^+]}{\Delta A(0) \bullet [BChl]} \tag{13}$$

The values of j_0 obtained by following the above described procedure from the carotenoid shift decays recorded in the presence of N2224-NTf_2, BMPyrr-NTf_2, c_1c_2Im-NTf_2, c_1c_2Im OTf, c_1c_2Im-BF_4 and Chol-Cl are shown in Fig. 5.

All the compounds tested, except Choline-Cl, are able to strongly enhance the dissipative ionic current, but the ILs containing the NTf_2^- anion do so at much lower concentrations. Interestingly, while N2224-NTf_2, BMPyrr-NTf_2, c_1c_2Im-NTf_2 gave fully reproducible results in repeated measurements, c_1c_2Im-BF_4 and c_1c_2Im-OTf showed a loss of activity over time (see Fig. S3). The BF_4^- anion, as reported by the manufacturer, tends to decompose when exposed to ambient humidity; apparently in our hands also the c_1c_2Im-OTf is an unstable compound.

3.3. The NTf_2^- anion strongly accelerates dissipative ion currents

The results summarized in Fig. 5 suggest that the NTf_2^- anion is

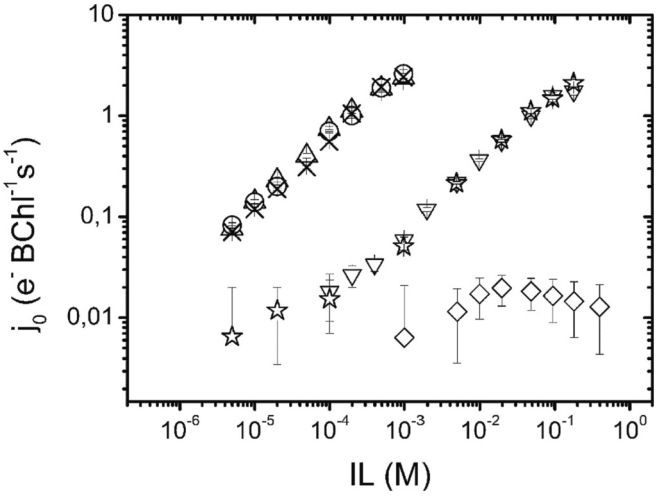

Fig. 5. Dependence of the ionic current j_0 on the molar concentration of N2224-NTf_2 (triangles), BMPyrr-NTf_2 (circles), c_1c_2Im-NTf_2 (crosses), c_1c_2Im-BF_4 (inverted triangles), c_1c_2Im-OTf (stars), Chol-Cl (diamonds).

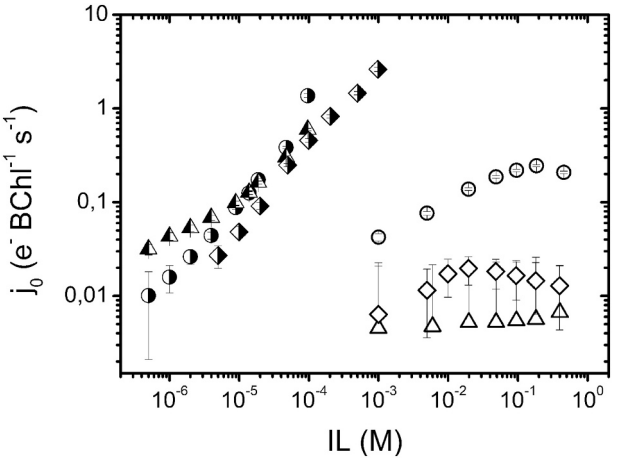

Fig. 6. The dependence of the ionic current j_0 on the molar concentration of BMPyrr-NTf$_2$ and BMPyrr-Cl (circles), c_1c_2Im-NTf$_2$ and c_1c_2Im-Cl (triangles), Chol-NTf$_2$ and Chol-Cl (diamonds). Half-filled and open symbols refer to the ILs with NTf_2^- or chloride anion, respectively.

responsible for a particularly effective dissipation of the membrane potential ΔΨ. In order to further corroborate this conclusion, we have examined the effect on the carotenoid shift signal of increasing concentrations of BMPyrr-Cl and c_1c_2Im-Cl, i.e. of ILs in which the chloride anion replaces NTf_2^-. As shown in Fig. 6, which compares the ionic current obtained in the presence of IL containing the same cation and the NTf_2^- or the Cl^- anion, the c_1c_2Im-Cl exerts a negligible effect on the membrane ionic current as compared to the control and BMPyrr-Cl results in a very limited progressive increase of j_0, but only at concentrations more than 3 orders of magnitude higher than BMPyrr-NTf$_2$.

The very weak increase of j_0 induced by BMPyrr-Cl, as compared to the much smaller effect in the presence of c_1c_2Im-Cl, could be explained by the longer alkyl chain of the BMPyrr$^+$ cation as compared to the $c_1c_2Im^+$ [44,45], in line with what reported by Liu et al. [9]. In fact these authors, working on chromatophores isolated from the closely related species *Rb. sphaeroides*, observed a decrease in the carotenoid band shift amplitude when the cationic alkyl chain of the IL 1-alkyl-3-methylimidazolium bromide lengthens. We also note that the j_0 values measured in the presence of high concentrations of BMPyrr-Cl (0.27–0.3 e^-BChl^{-1} s^{-1}) nicely agree with what evaluated by us in a previous work on Chr isolated from *Rb. sphaeroides* [8].

In order to further demonstrate the crucial role of the NTf_2^- anion in causing a dramatic increase of membrane permeability we examined the effect on j_0 of choline-NTf$_2$. As shown in Fig. 6, the values of j_0 as a function of choline-NTf$_2$ concentration are very close to those found in the presence of the other NTf$_2$-containing ILs, clearly indicating the high efficacy of this anion in dissipating the membrane potential.

3.4. The interaction of the NTf_2^- anion with the membrane is reversible

The above results indicate that the NTf_2^- anion is particularly effective in collapsing the membrane potential ΔΨ. To verify if the interaction of this anion with Chr vesicles is reversible, we adopted the following experimental scheme. Two aliquots (2 mL each) of Chrs suspended in 50 mM MOPS buffer, pH 7.3, were kept for 30 min in the dark in the presence/absence of 1 mM N2224-NTf$_2$, a concentration capable of inducing a rapid collapse of the carotenoid band shift (see Fig. 4). Subsequently both samples were extensively dialyzed against the same IL-free buffer (24 h, 3 × 500 mL, change every 8 h) before measuring the carotenoids band shift decay. As illustrated in Fig. S4, the sample incubated with 1 mM N2224-NTf$_2$ exhibits, after dialysis, the same carotenoid band shift kinetics as the control sample, indicating that N2224-NTf$_2$ has been removed. This implies that the interaction of the NTf_2^- anion with the Chr membrane is reversible.

3.5. Effect of ionic liquids on photosynthetic growth of Rb. Capsulatus

Some of the ILs tested on the Chr vesicles induce, at low concentrations, a rapid depolarization of the membrane potential upon single excitation of the RC, suggesting that they may be toxic to the bacterium. We therefore followed the photosynthetic growth of *Rb. capsulatus* in the presence of ILs. In agreement with what observed in chromatophores, the results show that the ILs containing NTf$_2$ are more effective at inhibiting growth. However, growth is completely suppressed only at concentrations significantly higher than those required to affect the decay of the membrane potential of chromatophores in single turnover flash (see Fig. S5 and Discussion).

4. Discussion

Time-resolved spectroscopic studies in chromatophores excited by a single actinic flash represent a useful method to investigate the effects of ionic liquids on the integrity of a biological membrane. All five initially tested ILs, N2224-NTf$_2$, BMPyrr-NTF$_2$, c_1c_2Im-NTf$_2$, c_1c_2Im-BF$_4$ and c_1c_2Im-OTf, were shown to be able to interact with the Chr membrane, inducing a more rapid dissipation of the membrane potential generated by the photoexcitation of the RC. In all cases, the carotenoid shift decay is clearly biphasic, with a fast phase increasing in amplitude at increasing concentration of the added IL. In order to account for this nonhomogeneous kinetics two models have been considered. In the first model, originally developed to explain a similar biphasic behavior of the carotenoid shift observed in the presence of ionophores in photosynthetic membrane vesicles [37,46,47], biphasicity was explained in terms of the statistical (Poissonian) distribution of permeating ions over the vesicle population, with the slow kinetic phase arising essentially from the fraction of the vesicle population lacking permeating ions. This model, resulting in Eq. (1), had been shown by us in a previous study [8] to describe accurately the effect of a set of ILs examined on the carotenoid shift decays. The second model was originally developed in charge-pulse relaxation studies of the transport kinetics of hydrophobic ions [39] and subsequently extended and adapted to describe the protonophoric activity of uncouplers in artificial [40] and native [48] membranes. This model explains the biphasicity of the membrane potential decay by considering the mechanism of the permeating species, which involves its adsorption at the water membrane interface, its translocation across the energy barrier of the membrane core, and its desorption into the aqueous opposite interface. Under appropriate assumptions such a mechanism leads to a biexponential decay of the membrane potential (Eq. (2)), with the fast decaying phase reflecting the translocation across the central barrier, and the slow process the exchange between the interfacial adsorption sites and solution, possibly limited by the diffusion rate in the unstirred aqueous layers facing the membrane [39].

When applied to the analysis of the carotenoid shift decays, the two models give access to different parameters characterizing the mechanism of IL permeation. The first, statistical model provides an estimate of the average number m of permeating ions per vesicle, of a rate constant k describing the ionic conductance induced by the IL, and of a rate constant k_l describing the intrinsic background ion leak of the membrane in the absence of ILs (see Table S1). At variance, the second model, allows to evaluate, by using Eqs. (9) and (10), the rate constant k_i determining the translocation of the ion across the membrane energy barrier and the total surface concentration of the ion adsorbed at the water-membrane interfaces (see Table 1). Although both models, i.e. Eq. (1) and (2), yield a comparably accurate fit of the carotenoid shift decays recorded for all the ILs at all the tested concentrations (see Fig. S1 and S2), the second model offers in our opinion a better interpretation of the observed behavior, because, besides being conceptually simpler, it results in more physically meaningful estimates of the parameters

characterizing the ion permeation. A first point concerns the strong increase of the rate constants k upon increasing the IL concentration which results by best fitting the carotenoid shift decays to Eq. (1). According to the statistical model k should be in principle concentration-independent, as found for a different set of ILs in a previous study [8] in which the statistical model was adopted. The only explanation for such a strong concentration dependence of the rate constant k of any individual ion would be that the IL perturbs progressively, at increasing concentration, the membrane structure and consequently the energetics governing ion permeation. This scenario is not easily reconcilable with the total reversibility of the IL effects on the decay of the carotenoid shift (see par. 3.4 of Results and Fig. S4). We notice that the rate constant values k_i obtained by adopting the second model (i.e. by fitting the whole set of data to Eq. (2)) exhibit a much more limited dependence upon the IL concentration, which may reflect milder changes in the membrane permeability associated with a progressive and substantial adsorption of the permeating ion (see below). A second point, disfavouring the statistical model, concerns the implications of the values obtained for the average number m of permeating ions per vesicle, which appears to increase, as expected, with concentration, but saturates at very small values (around 2) for all the ILs examined (see Table S1). It is useful to put this value in relation with the average surface of lipids forming the chromatophore vesicle. According to the model developed by Singharoy et al. [49], based on atomic force microscopy data and computer simulations, the average surface of the chromatophore vesicle is about 34,000 nm^2 (corresponding to an average internal diameter of 52 nm) and it is largely covered by proteins. By considering the reported number of 17,200 lipids per chromatophore [49] and assuming a mean surface area occupied by a phospholipid head of 0.64 nm^2 [50], the lipid component of the Chr membrane bilayer can be evaluated to occupy in fact approximately 5500 nm^2, i.e. about 16 % of the total chromatophore surface. A maximum average number of permeating ions per vesicle around 2, provided by the statistical model, and the estimate of 17,200 lipids per chromatophore [49] corresponds to a single permeating ion every 8600 lipids. It is difficult to understand that saturation in the average number of permeating ions is reached for such a large lipid domain in principle available for ion diffusion.

The model based on Eq. (2), yields estimates for the total number of ions adsorbed at the membrane-water interfaces, N_t. As expected, N_t increases at increasing IL concentrations (see Table 1) and exhibits a saturation behavior for all the IL examined. Such a saturation has been also observed in the case of hydrophobic ions permeating artificial bilayer membranes [39]. N_t saturates at values close to 5 pmoles·cm^{-2} (see Table 1). This value, assuming a mean surface area occupied by a phospholipid head of 0.64 nm^2 [50], and considering that lipids occupy about 16 % of the total chromatophore surface (see above), corresponds to approximately one ion adsorbed every 8 lipids at saturation. When comparing this estimate with the saturated m value of one ion every 8600 lipids predicted by the statistical model, it appears that the maximum surface density of ions interacting with the membrane predicted by the second model (calculated by using Eq. (10)), is about 3 orders-of-magnitude larger and, at variance with what predicted by the statistical model, corresponds to a physically meaningful value, well compatible with saturation of ion adsorption. Noteworthy, the estimated average domain of 8 lipid molecules per adsorbed ion, obtained from the N_t values, should be most likely further reduced. In chromatophores, in fact, the lipids bound to or interacting with membrane protein complexes [20,51,52] are supposed to be very rigid. Since a high mobility of the lipid molecules forming the bilayer is thought to be a strict requirement for ion permeation in all the molecular mechanisms proposed for passive ion diffusion through the membrane [53,54], the lipid regions of the Chr vesicle which can be effectively involved in ion adsorption and permeation will account for even less than 16 % of the total chromatophore surface.

When examining the N_t values obtained in ILs containing NTf_2 (N2224-NTf_2, BMPyrr-NTf_2, c_1c_2Im-NTf_2), more effective in collapsing the membrane potential $\Delta\Psi$, with those calculated for the less effective c_1c_2Im-BF_4 and c_1c_2Im-OTf, it appears that comparable N_t values are obtained in the latter at IL concentrations larger by more than one order-of-magnitude. This suggests that ILs containing NTf_2 are characterized by a much larger partition in the membrane phase. Table 1 shows that the same holds for the values of the rate constant k_i suggesting a lower energy barrier for intramembrane translocation of the $\Delta\Psi$ collapsing ion in ILs containing NTf_2.

The initial ion flux j_0, i.e. the membrane ionic current immediately after the actinic flash, accurately evaluated by means of Eqs. (12) and (13) from the best fitting parameters of Table 1, allows a model-independent comparison of the effectiveness of the different ILs examined in discharging the light-generated $\Delta\Psi$. As shown in Fig. 5, all the ILs raise the ionic current j_0 at sufficiently high concentrations, but the behavior observed for the NTf_2-containing ILs and c_1c_2Im-BF_4 or c_1c_2Im-OTf shows a clear distinction, being the former ILs effective in increasing j_0 at much lower concentrations. All these evidences point to a specific role played by the NTf_2^- anion. To verify if NTf_2 is mainly responsible for the strongly increased ionic current, we have examined and analyzed the carotenoid shift decay kinetics in the presence of BMPyrr-Cl and c_1c_2Im-Cl, i.e. in the presence of components, containing the same cations, in which Cl-anion replaces NTf_2^-. The j_0 values obtained (Fig. 6) clearly showed that, in the absence of NTf_2, the IL-induced increase of the ionic current is essentially negligible even at very high (100 mM) concentrations: in the case of BMPyrr-Cl a very weak increase of j_0 is detected only at such high concentrations and in the case of c_1c_2Im-Cl no ionic current increase is observed at all, as found in the presence of choline chloride (used as impermeant control). As a confirmation of the critical role of the NTf_2^- anion in rapidly dissipating the membrane potential, in the presence of Chol-NTf_2 essentially the same dependence of j_0 upon IL concentration, characterized by a large increase in ionic current at very low concentrations (Fig. 6), is found as for all other NTf_2-containing ILs.

Consistently with these findings, the NTf_2^- anion exhibits strong lipophilicity [55,56], suggesting that the energy cost for its permeation across the lipid bilayer is lower than that required by the other anions tested in the present study. Such a lipophilicity has been proposed to be a key feature in determining the anion cytotoxicity [55]. The analysis of the carotenoid shift decays in terms of Eqs. (2), (9) and (10) is in line with these conclusions, since, as mentioned above, NTf_2-containing ILs exhibit high k_i and N_t values at concentrations lower by more than one order-of-magnitude as compared to the other tested ILs (Table 1).

The fact that for the set of ILs examined a high effectiveness in collapsing the membrane potential is determined by the anionic moiety, being maximized for the NTf_2^- anion, suggests that the strong membrane adsorption (N_t) and rapid translocation (k_i) found for the NTf_2^- anion are to a large extent due to the positive membrane dipole potential of the membrane. This contribution to the total energy profile for ion interaction with lipid bilayers has been shown in fact to be critical in governing ion binding and permeation [57], leading to anions permeating the membrane much more readily than structurally analogue cations.

The maximum values of j_0 obtained are approximately equal to 3 $e^-Bchl^{-1}\ s^{-1}$ for N2224-NTf_2, BMPyrr-NTf_2 and c_1c_2Im-NTf_2 (see Fig. 5). In order to better compare the ionic current expressed in $e^-Bchl^{-1}\ s^{-1}$ with the currents measured in other membrane systems, the values of j_0 can be converted into electric current densities expressed in A m^{-2} [8]. This can be done on the basis of the average surface area occupied by a phospholipid head, approximately equal to 0.64 nm^2 [50], and of the molar ratio between lipids and BChl estimated equal to about 7 [49], in good agreement with the experimentally reported value of 5 ± 2 [41] previously employed by us for similar calculations [8]. By using these values and the charge of the electron (1.602 10^{-19}C) we can obtain the current densities of the lipid bilayer in the presence of the ILs tested. When the NTf_2^- anion is present at the concentration of 1 mM a current of approximately 0.21 A m^{-2} is found, as compared to 0.15 mA m^{-2} measured (on average) in control samples.

The effects of ILs on the photosynthetic growth curves of *Rb.*

capsulatus are qualitatively consistent with the acceleration of the membrane potential dissipation detected in chromatophores. However, to completely inhibit the photosynthetic growth, somewhat higher concentrations of ILs are required (Fig. S5). This is not surprising, since, being *Rb.capsulatus* a Gram-negative bacterium, it can be expected that the cell membrane is protected by the cell wall and the outer membrane against the direct interaction with ILs. Moreover, in a bacterial cell growing under photosynthetic conditions, the proton-motive force, which governs energy transduction and storage in vivo, is determined by the balance between the rate of cyclic electron transport and the consumption of the electrical (ΔΨ) and concentration (ΔpH) components due to ATP synthesis, active membrane transport, proton and ion leaks. A ΔΨ dissipating effect, like that induced by the ILs examined, tends to increase the rate of photoinduced electron flow and can in turn result in increased ΔpH, thus partially compensating for the loss of membrane potential [58]. Such a modulation of the protonmotive force can contribute to reduce the uncoupling effect of ILs.

5. Conclusions

The presented results show that the NTf_2^- anion rapidly permeates a native biological membrane, causing a rapid collapse of the transmembrane electrical potential difference. In view of the critical role played by ionic permeability of the membrane in all biological energy transducing and transport processes, we expect that NTf_2-containing ILs are potentially toxic in vivo.

In general, our analysis of the effects of different ILs on the ionic conductance of Chr membranes corroborates the notion that these vesicles, isolated from photosynthetic bacteria, are an ideal membrane system to investigate the interaction of charged chemical species with a native biological membrane and its consequences on passive ionic diffusion which regulates the level of the transmembrane electric potential difference. In such studies, chromatophores offer a number of remarkable advantages, among which: (a) they provide a relatively simple but totally integer membrane-protein system capable of energy transduction; (b) the huge amount of bioenergetic studies performed during the last decades has led to a detailed structural and functional characterization, including knowledge of the atomic-level structure of all the protein complexes involved in energy transduction, of their supramolecular organization, and of the electron and proton transport events which generate the electrical (ΔΨ) and pH (ΔpH) components of the protonmotive force; (c) the possibility of activating the RC photochemistry through short light pulses allows to elicit single turnovers of the energy transducing machinery; (d) the presence within antenna complexes of carotenoids undergoing an electrochromic shift in response to transmembrane electric fields provide an intrinsic molecular voltmeter which allows to monitor the single turnover generation of the transmembrane electrical potential and its subsequent dissipation determined by ionic currents without any a priori limitation in time resolution.

We have found that a model originally developed to investigate the transport of hydrophobic ions across artificial lipid membranes by charge pulse relaxation methods [39] accurately accounts for the biphasic kinetics of membrane potential dissipation in the presence of all the different ILs examined on a large range of concentrations. The model yields a consistent picture at the molecular level of the interaction of ILs whit the Chr membrane, providing information on the adsorption of the permeating ions at the membrane-solution interface and on the rapidity of ion translocation across the central potential energy barrier of the membrane. The knowledge of these parameters fully determines the ionic current through the membrane, and allows to compare the effectiveness of the examined ILs in dissipating the light-generated membrane potential. We have found that the NTf_2^- anion is responsible of the high effectiveness of a series of ILs in collapsing the membrane potential, independently of its cationic moiety, being characterized by strong adsorption at the membrane-water interfaces and fast translocation across the central energy barrier of the Chr membrane. The approach developed can be of help to evaluate the influence of other compounds produced by green chemistry on a native biological membrane and to understand the molecular basis of toxicity effects revealed by complementary in vivo studies.

CRediT authorship contribution statement

Tancredi Bin: Formal analysis, Investigation. **Giovanni Venturoli:** Methodology, Software, Writing – review & editing. **Anna Maria Ghelli:** Funding acquisition, Project administration. **Francesco Francia:** Conceptualization, Formal analysis, Investigation, Supervision, Writing – original draft.

Declaration of competing interest

Authors declare that they have no known competing financial interests or personal relationships that could have appeared to influence the work reported in this paper.

Acknowledgements

This study was supported by the Italian MIUR, grants RFO218 and RFO2019; T.B. is the recipient of a doctoral scholarship from the Italian MIUR, PON Project "Ricerca e Innovazione 2014-2020" (Code: DOT1303139; CUP: J35F21003050006). Authors are grateful to C. Samorì, P. Galletti and E. Tagliavini for helpful discussions. The *Rb. capsulatus* strain MT1131 was a generous gift from F. Daldal.

Appendix A. Supplementary data

Supplementary data to this article can be found online at https://doi.org/10.1016/j.bbamem.2024.184291.

References

[1] M.B. Shiflett, Commercial applications of ionic liquids, Springer Nature Switzerland, Cham. (2020), https://doi.org/10.1007/978-3-030-35245-5.
[2] S. Beil, M. Markiewicz, C.S. Pereira, P. Stepnowski, J. Thöming, S. Stolte, Toward the proactive Design of Sustainable Chemicals: ionic liquids as a prime example, Chem.Rev. 121 (2021) 13132–13173, https://doi.org/10.1021/acs.chemrev.0c01265.
[3] Li,W., Musa, D.A.R., Ahmad, N., Adil, M., Altimari U.S., Ibrahim, A.K., Alshehri, A. M., Riyahi, Y., Jaber, A.S., Kadhim, S.I., Rushchitc, A.A. and Aljuaid, M.O., 2023. Comprehensive review on the efficiency of ionic liquid materials for membrane separation and environmental applications, Chemosphere, 332, 138826. doi: https://doi.org/10.1016/j.chemosphere.2023.138826.
[4] J. Pesic, M. Watson, S. Papovic, M. Vranes, Ionic liquids: review of their current and future industrial applications and their potential environmental impact, Recent Pat. Nanotechnol. 15 (2021) 225–244, https://doi.org/10.2174/1872210513999190923121448.
[5] V. Thamke, P. Singh, S. Pal, M. Chaudhary, K. Kumari, I. Indra Bahadur, R. S. Varma, Current toxicological insights of ionic liquids on various environmental living forms, J.Env.Chem.Engineer. 10 (2022) 107303, https://doi.org/10.1016/j.jece.2022.107303.
[6] A.R.P. Goncalves, X. Paredes, A.F. Cristino, F.J.V. Santos, C.S.G.P. Queiros, Ionic liquids—a review of their toxicity to living organisms, Int. J. Mol. Sci. 22 (2021) 5612, https://doi.org/10.3390/ijms22115612.
[7] A. Benedetto, Room-temperature ionic liquids meet bio-membranes: the state-of-the-art, Biophys. Rev. 9 (2017) 309–320, https://doi.org/10.1007/s12551-017-0279-1.
[8] M. Malferrari, D. Malferrari, F. Francia, P. Galletti, E. Tagliavini, G. Venturoli, Ionic liquids effects on the permeability of photosynthetic membranes probed by the electrochromic shift of endogenous carotenoids, Biochim.Biophys.Acta 1848 (2015) 2898–2909, https://doi.org/10.1016/j.bbamem.2015.09.006.
[9] X.-L. Liu, M.-Q. Chen, Y.-L. Jiang, R.-Y. Gao, Z.-J. Wang, P. Wang, *Rhodobacter sphaeroides* as a model to study the ecotoxicity of 1-alkyl-3-methylimidazolium bromide, Front. Mol. Biosci. (2023), https://doi.org/10.3389/fmolb.2023.1106832.
[10] C.W. Mullineaux, L.-N. Liu, Membrane dynamics in phototrophic Bacteria, Annu. Rev. Microbiol. 74 (2020) 633–654, https://doi.org/10.1146/annurev-micro-020518-120134.
[11] B.I. Escher, M. Snozzi, K. Haberli, R.P. Schwarzenbach, A new method for simultaneous quantification of uncoupling and inhibitory activity of organic

pollutants in energy-transducing membranes, Env. Tox. Chem. 16 (1997) 405–414, https://doi.org/10.1002/etc.5620160303.
[12] N. Schweigert, R.W. Hunziker, B.I. Escher, R.I. Eggen, Acute toxicity of (chloro-) catechols and (chloro-)catechol-copper combinations in *Escherichia coli* corresponds to their membrane toxicity in vitro, Environ.Toxicol.Chem. 20 (2001) 239–247, https://doi.org/10.1002/etc.5620200203.
[13] R.J. Cogdell, N.W. Isaacs, A.A. Freer, J. Arrelano, T.D. Howard, M.Z. Papiz, A. M. Hawthornthwaite-Lawless, S. Prince, The structure and function of the LH2 (B800-850) complex from the purple photosynthetic bacterium *Rhodopseudomonas acidophila* strain 10050, Prog.Biophys.Mol.Biol. 68 (1997) 1–27, https://doi.org/10.1016/s0079-6107(97)00010-2.
[14] P. Qian, D.J.K. Swainsbury, T.I. Croll, P. Castro-Hartmann, G. Divitini, K. Sader, C. N. Hunter, Cryo-EM structure of the *Rhodobacter sphaeroides* light-harvesting 2 complex at 2.1 Å, Biochemistry 60 (2021) 3302–3314, https://doi.org/10.1021/acs.biochem.1c00576.
[15] J. Deisenhofer, O. Epp, K. Miki, R. Huber, H. Michel, X-ray structure analysis of a membrane protein complex. Electron density map at 3 Å resolution and a model of the chromophores of the photosynthetic reaction center from *Rhodopseudomonas viridis*, J. Mol. Biol. 180 (1984) 385–398, https://doi.org/10.1016/s0022-2836(84)80011-x.
[16] J.P. Allen, G. Feher, T.O. Yeates, H. Komiya, D.C. Rees, Structure of the reaction center from *Rhodobacter sphaeroides* R-26: the cofactors, Proc.Natl.Acad.Sci. USA 84 (1987) 5730–5734, https://doi.org/10.1073/pnas.84.16.5730.
[17] J.P. Allen, G. Feher, T.O. Yeates, H. Komiya, D.C. Rees, Structure of the reaction center from *Rhodobacter sphaeroides* R-26: the protein subunits, Proc.Natl.Acad.Sci. USA 84 (1987) 6162–6166, https://doi.org/10.1073/pnas.84.17.6162.
[18] L. Bracun, A. Yamagata, B.M. Christianson, M. Shirouzu, L.-N. Liu, Cryo-EM structure of a monomeric RC-LH1-PufX supercomplex with high-carotenoid content from *Rhodobacter capsulatus*, Structure 31 (2023) 318–328, https://doi.org/10.1016/j.str.2023.01.006.
[19] L. Esser, M. Elberry, F. Zhou, C.A. Yu, L. Yu, D. Xia, Inhibitor-complexed structures of the cytochrome bc1 from the photosynthetic bacterium *Rhodobacter sphaeroides*, J.Biol.Chem. 283 (2008) 2846–2857, https://doi.org/10.1074/jbc.M708608200.
[20] D.J.K. Swainsbury, F.R. Hawkings, E.C. Martin, S. Musiał, J.H. Salisbury, P. J. Jackson, D.A. Farmer, M.P. Johnson, C.A. Siebert, A. Hitchcock, C.N. Hunter, Cryo-EM structure of the four-subunit *Rhodobacter sphaeroides* cytochrome *bc*1 complex in styrene maleic acid nanodiscs, Proc.Natl.Acad.Sci. USA 120 (2023) e2217922120, https://doi.org/10.1073/pnas.2217922120.
[21] E. Morales-Rios, M.G. Montgomery, Andrew G.W. Leslie, A.G. W., J.E. Walker, Structure of ATP synthase from *Paracoccus denitrificans* determined by X-ray crystallography at 4.0 Å resolution, Proc.Natl.Acad.Sci. USA 112 (2015) 13231–13236, https://doi.org/10.1073/pnas.1517542112ù.
[22] J.B. Jackson, Bacterial photosynthesis, in: C. Anthony (Ed.), Bacterial Energy Transduction, Academic Press, London, 1988, pp. 317–375.
[23] A.R. Crofts, The modified Q-cycle: a look back at its development and forward to a functional model, Biochim. Biophys. Acta 1862 (2021) 148417, https://doi.org/10.1016/j.bbabio.2021.148417.
[24] P. Mitchell, Chemiosmotic coupling in oxidative and photosynthetic phosphorylation, Biol. Rev. 41 (1966) 445–502, https://doi.org/10.1111/j.1469-185X.1966.tb01501.x.
[25] D.G. Nicholls, S.J. Ferguson, Bioenergetics, fourth ed., Academic Press, 2013 https://doi.org/10.1016/C2010-0-64902-9.
[26] N.G. Holmes, C.N. Hunter, R.A. Niederman, A.R. Crofts, Identification of the pigment pool responsible for the flash-induced carotenoid band shift in Rhodopseudomonas sphaeroides chromatophores, FEBS Lett. 115 (1980) 43–48, https://doi.org/10.1016/0014-5793(80)80723-X.
[27] J.B. Jackson, A.R. Crofts, The high energy state in chromatophores from Rhodopseudomonas sphaeroides, FEBS Lett. 4 (1969) 185–189, https://doi.org/10.1016/0014-5793(69)80230-9.
[28] H.-G. Koch, O. Hwang, F. Daldal, Isolation and characterization of Rhodobacter capsulatus mutants affected in cytochrome cbb3 oxidase activity, J. Bacteriol. 180 (1998) 969–978, https://doi.org/10.1128/jb.180.4.969-978.1998.
[29] R.K. Clayton, Spectroscopic analysis of bacteriochlorophylls in vitro and in vivo, Photochem. Photobiol. 5 (1966) 669–677, https://doi.org/10.1111/j.1751-1097.1966.tb05813.x.
[30] W.P. Barz, F. Francia, G. Venturoli, B.A. Melandri, A. Verméglio, D. Oesterhelt, Role of PufX protein in photosynthetic growth of Rhodobacter sphaeroides. 1. PufX is required for efficient light-driven electron transfer and photophosphorylation under anaerobic conditions, Biochemistry 34 (1995) 15235–15247, https://doi.org/10.1021/bi00046a032.
[31] J.R. Bowyer, S.W. Meinhardt, G.V. Tierney, A.R. Crofts, Resolved difference spectra of redox centers involved in photosynthetic electron flow in Rhodopseudomonas capsulata and Rhodopseudomonas sphaeroides, Biochim. Biophys. Acta 635 (1981) 167–186, https://doi.org/10.1016/0005-2728(81)90016-5.
[32] E.H. Evans, A.R. Crofts, In situ characterisation of photosynthetic electron transport in Rhodopseudomonas capsulata, Biochim. Biophys. Acta 357 (1974) 89–102, https://doi.org/10.1016/0005-2728(74)90115-7.
[33] J.B. Jackson, P.L. Dutton, The kinetic and redox potentiometric resolution of the carotenoid shifts in Rhodopseudomonas spheroides chromatophores: their relationship to electric field alterations in electron transport and energy coupling, Biochim. Biophys. Acta 325 (1973) 102–113, https://doi.org/10.1016/0005-2728(73)90155-2.
[34] L.A. Drachev, M.D. Mamedov, A.Y. Mulkidjanian, A.Y. Semenov, V.P. Shinkarev, M.I. Verkhovsky, Phase II of carotenoid bandshift is mainly due to the electrogenic protonation of the secondary quinone acceptor, FEBS Lett. 233 (1988) 315–318, https://doi.org/10.1016/0014-5793(88)80450-2.
[35] E.G. Glaser, A.R. Crofts, A new electrogenic step in the ubiquinol:cytochrome c2 oxidoreductase complex of Rhodopseudomonas sphaeroides, Biochim. Biophys. Acta 766 (1984) 322–333, https://doi.org/10.1016/0005-2728(84)90248-2.
[36] J. Symersky, D. Osowsky, D.E. Walters, D.M. Mueller, Oligomycin frames a commondrug-binding site in the ATP synthase, Proc. Natl. Acad. Sci. U. S. A. 109 (2012) 13961–13965, https://doi.org/10.1073/pnas.1207912109.
[37] R. Schmid, W. Junge, Current-voltage studies on the thylakoid membrane in the presence of ionophores, Biochim. Biophys. Acta 394 (1975) 76–92, https://doi.org/10.1016/0005-2736(75)90206-0.
[38] K.-I. Takamiya, P.L. Dutton, The influence of transmembrane potentials of the redox equilibrium between cytochrome c2 and the reaction center in Rhodopseudomonas sphaeroides chromatophores, FEBS Lett. 80 (1977) 279–284, https://doi.org/10.1016/0014-5793(77)80457-2.
[39] R. Benz, P. Läuger, K. Janko, Transport kinetics of hydrophobic ions in lipid bilayer membranes. Charge-pulse relaxation studies, Biochim. Biophys. Acta 455 (1976) 701–720, https://doi.org/10.1016/0005-2736(76)90042-0.
[40] R. Benz, S. McLaughlin, The molecular mechanism of action of the proton ionophore FCCP (carbonylcyanide p-trifluoromethoxyphenylhydrazone), Biophys. J. 41 (1983) 381–398, https://doi.org/10.1016/S0006-3495(83)84449-X.
[41] R. Casadio, G. Venturoli, B.A. Melandri, Evaluation of the electrical capacitance in biological membranes at different phospholipid to protein ratios, Eur. J. Biophys. 16 (1988) 243–253, https://doi.org/10.1007/BF00261266.
[42] O.S. Andersen, M. Fuchs, Potential energy barriers to ion transport within lipid bilayers. Studies with tetraphenylborate, Biophys. J. 15 (1975) 795–830, https://10.1016/S0006-3495(75)85856-5.
[43] N.P.J. Cotton, A.J. Clark, J.B. Jackson, Changes in membrane ionic conductance, but not changes in slip, can account for the non-linear dependence of the electrochemical proton gradient upon the electron-transport rate in chromatophores, Eur. J. Biochem. 142 (1984) 193–198, https://doi.org/10.1111/j.1432-1033.1984.tb08269.x.
[44] V.K. Sharma, R. Mukhopadhyay, Deciphering interactions of ionic liquids with biomembrane, Biophys.Rev. 10 (2018) 721–734, https://doi.org/10.1007/s12551-018-0410-y.
[45] S. Kumar, H.A. Scheidt, N. Kaur, T.S. Kang, G.K. Gahlay, D. Huster, V.S. Mithu, Effect of the alkyl chain length of amphiphilic ionic liquids on the structure and dynamics of model lipid membranes, Langmuir 35 (2019) 12215–12223, https://doi.org/10.1021/acs.langmuir.9b02128.
[46] H. Lill, G. Althoff, W. Junge, Analysis of ionic channels by a flash spectrophotometric technique applicable to thylakoid membranes: CF0, the proton channel of the chloroplast ATP synthase, and for comparison, gramicidin, J. Membrane Biol. 98 (1987) 69–78, https://doi.org/10.1007/BF01871046.
[47] G. Althoff, G. Schönknecht, W. Junge, Gramicidin in chromatophores of Rhodobacter sphaeroides, Eur. Biophys. J. 19 (213) (1991) 216, https://doi.org/10.1007/BF00196347.
[48] B.I. Escher, R. Hunziker, R.P. Schwarzenbach, J.C. Westall, Kinetic model to describe the intrinsic uncoupling activity of substituted phenols in energy transducing membranes, Environ. Sci. Technol. 33 (1999) 560–570, https://doi.org/10.1021/es980545h.
[49] A. Singharoy, C. Maffeo, C.H. Delgado-Magnero, D.J.K. Swainsbury, M. Sener, U. Kleinekathöfer, J.W. Vant, J. Nguyen, A. Hitchcock, B. Isralewitz, I. Teo, D. E. Chandler, J.E. Stone, J.C. Phillips, T.V. Pogorelov, M.I. Mallus, C. Chipot, Z. Luthey-Schulten, D.P. Tieleman, C.N. Hunter, K. Schulten, Atoms to phenotypes: molecular design principles of cellular energy metabolism, Cell 179 (2019), https://doi.org/10.1016/j.cell.2019.10.021, 1098-1011.
[50] F. Gubellini, F. Francia, P. Turina, D. Lévy, G. Venturoli, B.A. Melandri, Heterogeneity of photosynthetic membranes from Rhodobacter capsulatus: size dispersion and ATP synthase distribution, Biochim. Biophys. Acta 1767 (2007) 1340–1352, https://doi.org/10.1016/j.bbabio.2007.08.007.
[51] M. Dezi, F. Francia, A. Mallardi, G. Colafemmina, G. Palazzo, G. Venturoli, Stabilization of charge separation and cardiolipin confinement in antenna–reaction center complexes purified from Rhodobacter sphaeroides, Biochim. Biophys. Acta 1767 (2007) 1041–1056, https://doi.org/10.1016/j.bbabio.2007.05.006.
[52] S. Nagatsuma, K. Gotou, T. Yamashita, L.-J. Yu, J.-R. Shen, M.T. Madigan, Y. Kimura, Z.-Y. Wang-Otomo, Phospholipid distributions in purple phototrophic bacteria and LH1-RC core complexes, Biochim. Biophys. Acta 1860 (2019) 461–468, https://doi.org/10.1016/j.bbabio.2019.04.001.
[53] I. Vorobyov, T.E. Olson, J.H. Kim, R.E. Koeppe II, O.S. Andersen, W. Toby, T. W. Allen, Ion-induced defect permeation of lipid membranes, Biophys. J. 106 (2014) 586–597, https://doi.org/10.1016/j.bpj.2013.12.027.
[54] A. Fathizadeh, R. Ron Elber, Ion permeation through a phospholipid membrane: transition state, path splitting, and calculation of permeability, J. Chem. Theory Comput. 15 (2019) 720–730, https://doi.org/10.1021/acs.jctc.8b00882.
[55] S. Stolte, J. Arning, U. Bottin-Weber, M. Matzke, F. Stock, K. Thiele, M. Marc Uerdingen, U. Welz-Biermann, B. Jastorff, J. Johannes Ranke, Anion effects on the cytotoxicity of ionic liquids, Green Chem. 8 (2006) 621–629, https://doi.org/10.1039/B602161A.
[56] S. Stolte, J. Arning, U. Bottin-Weber, A. Müller, W.-R. Pitner, U. Welz-Biermann, B. Johannes Jastorff, J. Ranke, Effects of different head groups and functionalised side chains on the cytotoxicity of ionic liquids, Green Chem. 9 (2007) 760–776, https://doi.org/10.1039/B615326G.
[57] R.F. Flewelling, W.L. Hubbel, The membrane dipole potential in a total membrane potential model. Applications to hydrophobic ion interactions with membranes, Biophys. J. 49 (1986) 541–552, https://doi.org/10.1016/s0006-3495(86)83664-5.
[58] R. Casadio, A. Baccarini Melandri, D. Zannoni, B.A. Melandri, Electrochemical proton gradient and phosphate potential in bacterial chromatophores, FEBS Lett. 49 (1974) 203–207, https://doi.org/10.1016/0014-5793(74)80512-0.